Myocardial First-Pass Perfusion: Influence of Spatial Resolution and Heart Rate on the Dark Rim Artifact

Antonella Meloni,[1]* Nidal Al-Saadi,[2] Geir Torheim,[3] Nadja Hoebel,[4] H. Glenn Reynolds,[5] Daniele De Marchi,[1] Vincenzo Positano,[1] Silvia Burchielli,[1] and Massimo Lombardi[1]

Myocardial perfusion images can be affected by the dark rim artifact. This study aimed to evaluate the effects of the spatial resolution and heart rate on the transmural extent of the artifact. Six pigs under anesthesia were scanned at 1.5T using an echo-planar imaging/fast gradient echo sequence with a nonselective saturation preparation pulse. Three short-axis slices were acquired every heart beat during the first pass of a contrast agent bolus. Two different in-plane spatial resolutions (2.65 and 3.75 mm) and two different heart rates (normal and tachycardia) were used, generating a set of four perfusion scans. The percentage drop of signal in the subendocardium compared to the epicardium and the transmural extent of the artifact were extracted. Additionally, the signal-to-noise and the contrast-to-noise ratios were evaluated. The signal drop as well as the width of the dark rim artifact increased with decreased spatial resolution and with increased heart rates. No significant slice-to-slice variability was detected for signal drop and width of the rim within the four considered groups. signal-to-noise ratio (SNR) and contrast-to-noise ratio (CNR) ratios decreased with increasing spatial resolution. In conclusion, low spatial and temporal resolution could be correlated with increased extent of the dark-rim artifact and with lower SNR and CNR. Magn Reson Med 66:1731–1738, 2011. © 2011 Wiley Periodicals, Inc.

Key words: myocardial perfusion; dark rim artifact; spatial resolution; heart rate

INTRODUCTION

Coronary artery disease (CAD) remains one of the leading causes of morbidity and mortality in developed countries. As a decrease in myocardial perfusion represents the first effect of occluding coronary artery disease, the early detection of myocardial perfusion abnormalities is the key factor in the optimal management of patients with suspected coronary artery disease and it could potentially reduce the rate of fatal myocardial infarctions (1).

In the clinical setting, the measurements of myocardial perfusion are usually performed with single-photon emission computed tomography (SPECT) (2) or with positron emission tomography (PET) (3,4). However, single-photon emission computed tomography imaging has a rather low-spatial resolution, delivers a significant dose of ionizing radiation, which is not quantitative, and suffers from soft tissue attenuation artifacts (5). Positron emission tomography has higher sensitivity and specificity than single-photon emission computed tomography (6,7) but is burdened by its limited availability.

Thanks to technical developments, magnetic resonance imaging (MRI) has emerged as a valid noninvasive alternative to nuclear techniques (8,9). First-pass perfusion MRI acquires a series of T_1-weighted images during the passage of a contrast bolus through the heart (10,11). Recent clinical studies have shown that MRI compares quite favorably with nuclear medicine (12,13) and has higher diagnostic accuracy for detection of significant coronary artery disease (14). However, myocardial first-pass perfusion imaging is burdened with a variety of artifacts, which might make confident assessment difficult. The most important and significant artifact appears at the border between the myocardium and the left ventricle (LV) cavity and has been termed dark rim artifact (DRA). It shows a hypointense signal and can visually resemble a subendocardial perfusion defect, or it could overlay a delayed wash-in of contrast agent during a first-pass perfusion study, which occurs with coronary artery stenosis. By mimicking or obscuring a perfusion defect, DRAs unavoidably affect both sensitivity and specificity of a perfusion study. Furthermore, these artifacts can have an important impact in calculating semiquantitative and quantitative parameters derived from signal intensity curves. Many factors have been attributed to cause this artifact such as susceptibility (15), spatial resolution (Gibbs ringing) (16), and motion effects (17). Most likely, the DRA is a combination of some or all of these factors (18).

The purpose of this study was to evaluate the influence of spatial resolution and heart rate on the transmural extent of the dark-rim artifact, signal-to-noise ratio (SNR), and contrast-to-noise ratio (CNR). Moreover, the potential presence of a slice-to-slice variability for the extension of the dark rim was explored.

MATERIALS AND METHODS

Animal Model

In vivo experiments were performed on six adult, healthy farm pigs (weight 32.5 ± 0.8 kg, range 30–34 kg).

[1]Fondazione G. Monasterio CNR-Regione Toscana and Institute of Clinical Physiology, Pisa, Italy.

[2]Heart Institute Berlin, Berlin, Germany.

[3]GE-Healthcare, Oslo, Norway.

[4]Kendle GmbH, Munich, Germany.

[5]GE Healthcare, Milwaukee, Wisconsin.

*Correspondence to: Antonella Meloni, Fondazione G. Monasterio CNR-Regione Toscana and Institute of Clinical Physiology, Via Moruzzi, 1 - 56124 Pisa, Italy. E-mail: antonella.meloni@ifc.cnr.it

Anesthesia was induced by tiletamine–zolazepam (10 mg/kg) and atropine (0.05 mg/kg) and was maintained by propofol (5 mg/kg/h). Endotracheal intubation was performed using a 6.5-mm tube. Ventilation was assured through the study by a mechanical ventilator (Siemens Servo-ventilator). An i.v. line was inserted into an ear vein, and the size of the canulla was chosen as large as possible (≥ 20 gauge) to allow for high-speed injection of contrast agent. The respirator was turned-off during first-pass imaging to minimize motion artifacts. Heart rate was monitored continuously and adjusted by using pharmacological intervention (dobutamine, atropine, and atenolol). Care was taken to avoid any drug with known direct vasodilating effect on coronary arteries. The animals were sacrificed by injecting potassium chloride (KCL).

The study was approved by the internal Ethical Committee of the C.N.R., Institute of Clinical Physiology—Pisa, Italy.

MRI

MRI was performed using a GE Excite HD 1.5T scanner (GE Healthcare, Milwaukee). An 8-channel cardiac coil was used for signal reception. Vector ECG was used to trigger all cardiac pulse sequences.

Myocardial first-pass studies were performed using the echo-planar imaging (EPI)/fast gradient echo (FGRE)-based sequence CASH2 (CAlibration Slice using Hybrid acquisition, version 2). The imaging parameters for CASH2 included a 90° nonselective saturation preparation pulse, chemical shift fat suppression, echo time (TE) 1.0 ms, repetition time (TR) 6.0 ms, flip angle (FA) 25°, Echo Train Length 4, array spatial sensitivity encoding technique (ASSET) factor 2, bandwidth ±125 kHz, number of excitations (NEX) 1, phase field of view (FOV) 1, matrix 128 × 128, and slice thickness 8 mm (Fig. 1). Three adjacent short axis slices (in the order: apical, basal, and medium) were acquired every heartbeat. A trigger delay of 15 ms after the R wave and an acquisition window of 336 ms (112 ms for each slice: 22 ms for saturation preparation and fat suppression pulses plus 90 ms for image acquisition) were chosen to minimize the effect of the cardiac motion. Images were acquired during and after a bolus injection of 0.075 mmol/kg of Omniscan™ Injection (gadolinium complex of diethylenetriamine pentaacetic acid bismethylamide, GE Healthcare AS, Oslo, Norway) with a power injector. The injection rate was adapted to an injection time of 3 s. Omniscan Injection was followed by a flush of 5 mL of saline using the same rate as for the contrast agent.

First-pass perfusion scans were performed using two different in-plane spatial resolutions (high-spatial resolution = 2.65 mm: group HRes and low-spatial resolution = 3.75 mm: group LRes) and two different heart rates (normal resting heart rate = 68 ± 6 bpm: rest group and tachycardia = 107 ± 10 bpm: tachycardia group), resulting in a set of four perfusion scans (HRes-rest, HRes-tachycardia, LRes-rest, and LRes-tachycardia) acquired in each pig. The two different spatial resolutions were obtained by adjusting the FOV (FOV = 340 mm for high-spatial resolution and FOV = 480 mm for low-spatial resolution), while heart rates were adjusted by pharmaceutical intervention, as described in the animal model
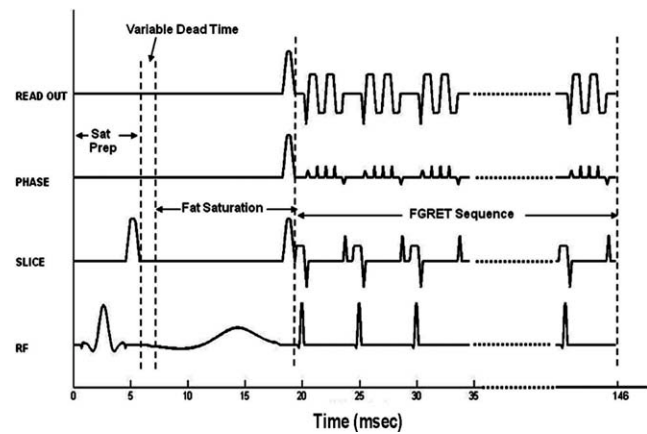

FIG. 1. Schematic diagram of the pulse sequence utilized: CASH2 (CAlibration Slice using Hybrid Acquisition) 2nd version.

section. The order of the four scans was chosen randomly within each pig. Time elapsing between two injections in the same pig was 60 min. Image data were transferred to a remote workstation for offline analysis.

Before each first-pass perfusion scan, dry scans without injection of contrast agent were performed to check image quality and presence of artifacts.

Image Analysis

The perfusion scans were presented in random order to an expert operator who performed the analysis blinded as to the resolution and heart rate. A previously validated tool (HIPPO PERF®) (19,20) was used. Analysis was performed on image frames where the DRA was most prominent. The horizontal (frequency encoding direction crossing the septal and lateral myocardial wall) and vertical (phase encoding direction crossing the anterior and inferior myocardial wall) signal intensity profiles (1 pixel width) were extracted (Figs. 2 and 3). The profiles were evaluated relative to the percentage drop of signal in the subendocardium compared to the signal intensity of the epicardium. The transmural extent of the dark rim was measured and expressed in percent of total myocardial wall thickness,. Hence, six measurements (two profiles × three slices) were performed for each perfusion scan, and their mean was used to characterize the scan.

The operator also identified the frame with the LV signal peak by extracting the signal versus time curve in the LV center.

The myocardial signal-to-noise ratio was evaluated by objective pixel quantification as the ratio between the mean signal calculated within a region of interest (ROI) and the standard deviation (SD) calculated in a large ROI in the image background, free of image artifacts. SD was corrected taking into account the Rician distribution of MR noise and the phased array coils geometry (21,22).

The CNR was evaluated between the basal myocardial signal (i.e. without presence of contrast medium) and the myocardial signal post contrast using the equation:

$$\mathrm{CNR} = \frac{|S_\mathrm{C} - S_\mathrm{B}|}{\frac{1}{2}(SD_\mathrm{bkC} + SD_\mathrm{bkB})}$$
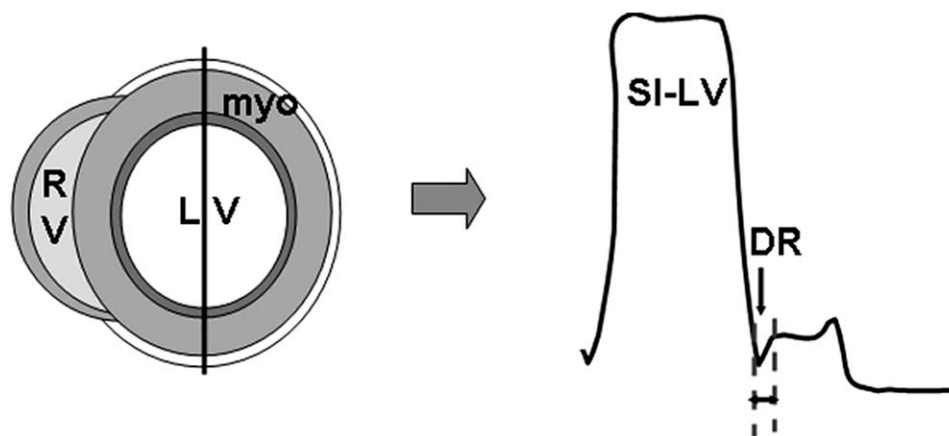
FIG. 2. Method used to extract signal intensity profiles. The user positions a vertical (as in figure) or horizontal line in the image, and the software generates the corresponding signal intensity profile along the line. LV: left ventricle, RV: right ventricle, myo: myocardium, DR: signal drop demonstrating the dark rim, and SI-LV: signal intensity of the left ventricular cavity.

where $|S_C - S_B|$ was the absolute difference between basal signal and the signal evaluated in one frame acquired after the 90% of signal rise due contrast pass. SD_{bkC} and SD_{bkB} were the signal SD calculated in a large ROI, free of image artifacts, in the image background, for basal and contrast enhanced images, respectively. SDs were corrected for the noise statistics as for SNR evaluation.

Both SNR and CNR were evaluated in anterior, septal, inferior, and lateral segments in all slices. Mean values across all segments were taken.

Statistical Analysis

All data were analyzed using SPSS version 13.0 and JMP version 8 statistical packages. Continuous variables were described as mean ± SD.

Paired Student's *t*-tests were performed to detect significant differences between groups using the following generalized hypothesis: H_0: group HRes-rest − group LRes-tachycardia = 0 versus H_A: group HRes-rest − group LRes-tachycardia < 0. The Bonferroni correction was used for multiple comparisons.

For each group, one-way repeated measures analysis of variance was used to evaluate if there was a significant difference in the extension of the DRA among the cardiac slices.

In all tests, a $P < 0.05$ was considered statistically significant.

RESULTS

Perfusion studies were successfully performed in all six pigs.

The mean heart rate was pointedly different for rest and tachycardia groups ($P = 0.001$) but not significantly different for HRes and LRes groups (83.2 ± 19.6 bpm versus 89.5 ± 21.9 bpm; $P = 0.304$).

Dark Rim

The most prominent DRA was detected on image frames shortly after the LV signal peak. In particular, the mean

time after the LV signal peak was 1.17 ± 0.43 s for the rest group and 0.89 ± 0.41 s for the tachycardia group.

The percentage of signal drop at the endocardium with the reference being the signal in the epicardial myocardium did not show a significant difference between HRes and LRes groups (27.1 ± 7.1% versus 33.2 ± 8.5%; $P = 0.084$) (Fig. 4a, left). The percentage of signal drop at the endocardium with the reference being the signal in the epicardial myocardium was significantly lower in the rest group than in the tachycardia group (27.0 ± 8.1% versus 33.0 ± 6.0%; $P = 0.019$) (Fig. 4a, center). The smallest signal drop was found in the HRes-rest group (21.1 ± 11.8%) and the largest one in the LRes-tachycardia group (35.0 ± 11.3%). The signal drop in HRes-tachycardia and LRes-tachycardia groups was 31.6 ± 7.8% and 32.1 ± 9.7, respectively. No significant differences were detected between the four groups (Fig. 4a, right).

The width of the dark rim was significantly bigger in the LRes group than in the HRes group (55.9 ± 13.2% of myocardial thickness versus 25.2 ± 7.9% of myocardial thickness; $P < 0.0001$) (Fig. 4b, left). The mean dark rim width in the LRes group was 2.2 times larger than in the HRes group. The dark rim was significantly wider in the tachycardia group than in the rest group (53.1 ± 7.2% of myocardial thickness versus 24.5 ± 8.7% of myocardial thickness; $P < 0.0001$) (Fig. 4b, center). The width of the rim was smaller in the HRes-rest group (6.9 ± 5.3% of myocardial thickness), followed by the HRes-tachycardia (41.3 ± 7.6% of myocardial thickness) and LRes-rest groups (46.1 ± 14.9% of myocardial thickness), whereas the LRes-tachycardia group showed the widest rim (66.0 ± 16.1% of myocardial thickness) (Fig. 4b, right). The difference in the width of the dark rim was not statistically significant only between HRes-tachycardia and LRes-rest groups.

Slice-to-Slice Variability of the Dark Rim Artifact

No significant slice-to-slice variability was detected for signal drop and width of the rim (expressed both as

HRes-rest   **HRes-tachycardia**   **LRes-rest**   **LRes-tachycardia**

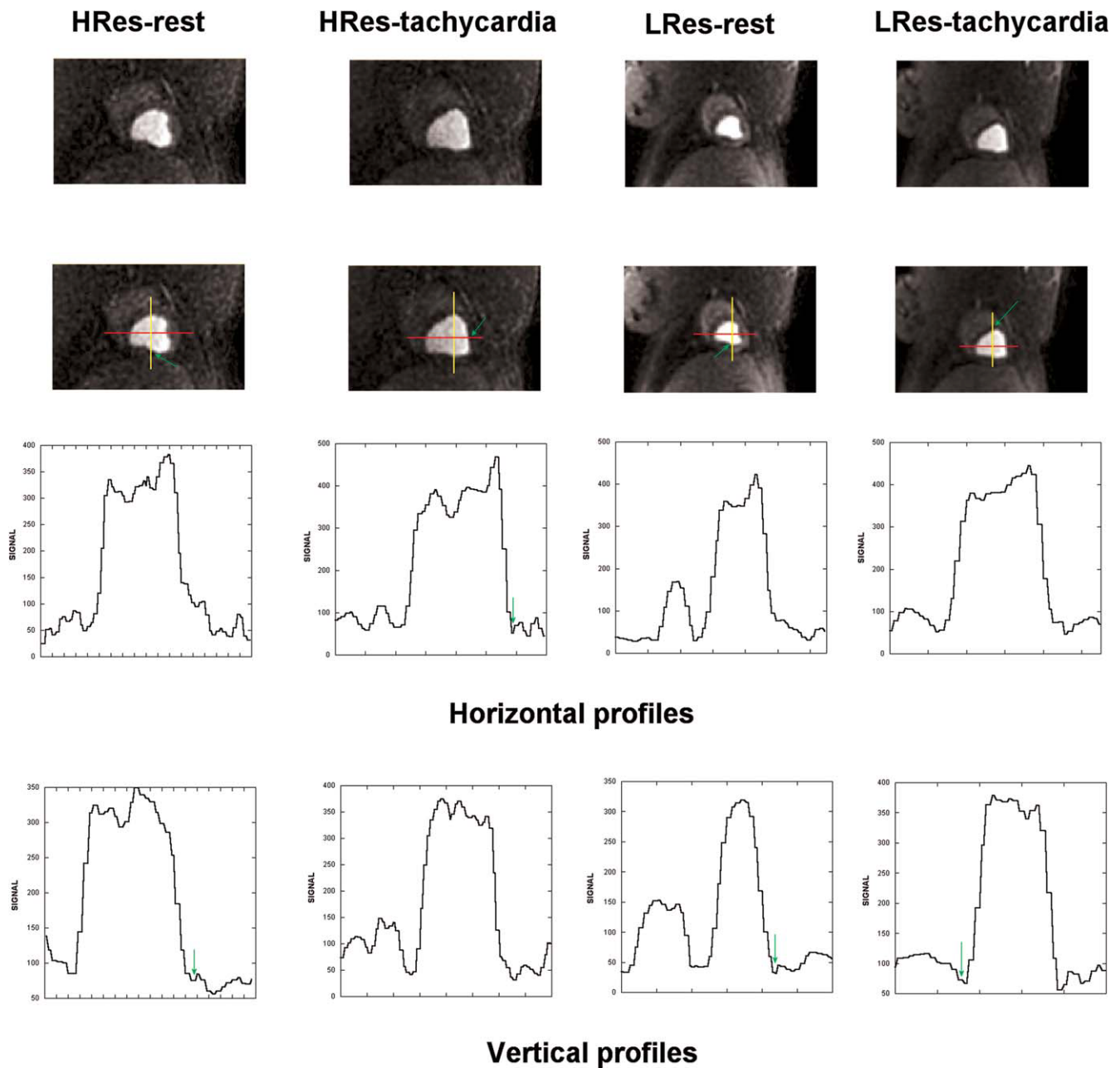**Horizontal profiles**

Vertical profiles

FIG. 3. Representative example of real data analysis (Pig #5, medium slice). From top to bottom: MR images, traced horizontal and vertical lines, horizontal profiles, and vertical profiles. Green arrows indicate the presence of a dark rim and the corresponding signal drop.

percent of total myocardial wall thickness and in mm) within the four considered groups (Table 1).

SNR and CNR

At precontrast, the SNR was significantly higher in the LRes group than in the HRes group (12.2 ± 5.1 versus 5.2 ± 2.9; $P < 0.0001$) and in the rest group than in the tachycardia group (10.3 ± 6.3 versus 7.2 ± 3.9; $P < 0.0001$) (Fig. 5a). The smallest SNR was found in the HRes-tachycardia group (3.9 ± 1.1) and the largest one in the LRes-rest group (13.9 ± 6.2). The SNR in HRes-rest and LRes-tachycardia groups was 6.6 ± 3.7

and 10.5 ± 2.9, respectively. Significant differences were found between all pairs (Fig. 5a, right). At peak contrast, the SNR was significantly higher in the LRes group than in the HRes group (29.6 ± 13.4 versus 13.9 ± 5.3; $P < 0.0001$), and no significant difference was detected between rest and tachycardia groups (20.7 ± 14.2 versus 22.9 ± 11.4; $P = 0.09$) (Fig. 5b). The smallest SNR was found in the HRes-rest group (13.1 ± 5.1) and the largest one in the LRes-tachycardia group (31.0 ± 9.8). The SNR in HRes-tachycardia and LRes-rest groups was 14.8 ± 5.4% and 28.2 ± 16.3, respectively. No significant differences were detected between LRes-rest and LRes-tachycardia groups and neither between HRes-rest
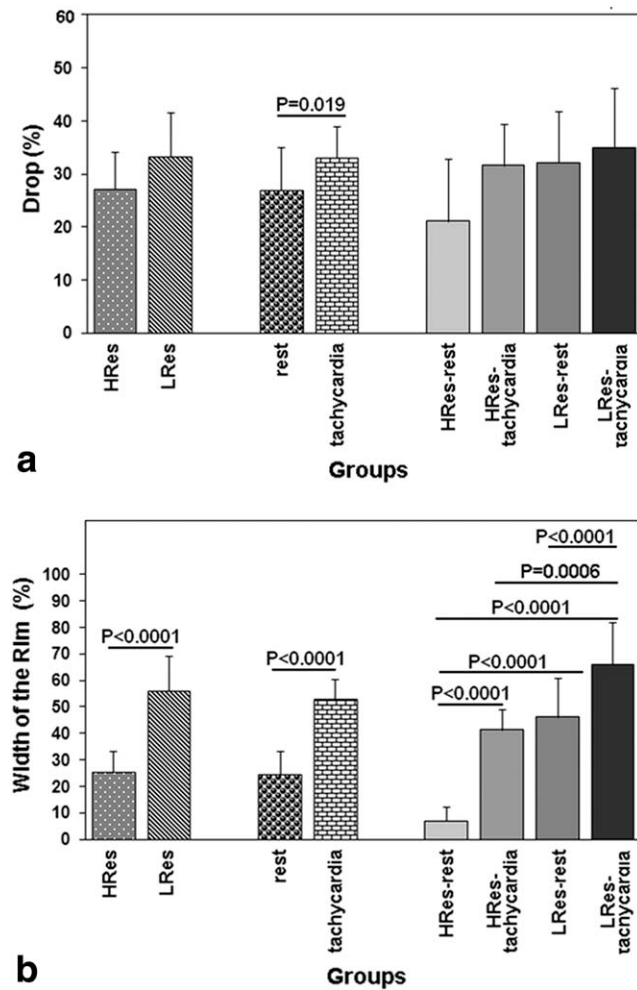
FIG. 4. **a**: Mean signal drop in percent in HRes and LRes groups (left), in normal and tachycardia groups (center) and in the four separate groups (right). **b**: Mean width of the dark rim in HRes and LRes groups (left), in normal and tachycardia groups (center), and in the four separate groups (right). The SD is reported. The horizontal lines indicate a significant difference between two groups and the correspondent *P* values are indicated.

and HRes-tachycardia groups (Fig. 5b, right). The SNR at peak contrast was significantly higher than the SNR at precontrast in all groups ($P < 0.0001$).

The CNR between pre- and peak-contrast images was significantly higher in the LRes group than in the HRes group (14.9 ± 4.3 versus 8.6 ± 4.1; $P < 0.0001$) and in the tachycardia group than in the rest group (13.4 ± 5.6 versus 10.1 ± 4.3; $P < 0.0001$) (Fig. 6). Among the four sets, the highest CNR was detected in the LRes-tachycardia group (16.9 ± 4.0) and the lowest in the HRes-rest group (7.2 ± 2.7). The CNR in HRes-tachycardia and LRes-rest group was $9.9 \pm 4.8\%$ and 12.8 ± 3.6, respectively. Significant differences were detected between all pairs, except for the pair constituted by HRes-tachycardia and LRes-rest groups (Fig. 6, right).

DISCUSSION

The evaluation of myocardial ischemia relies on the detection of reduced perfusion. MRI allows an analysis of myocardial perfusion by the use of the first pass of a T_1-shortening contrast agent bolus (10,11,23). Severe ischemia results in a long-lasting hypoenhancement during the complete first pass of the contrast agent through the myocardium. Moderate ischemia occurs as a transient hyopoenhancement of the subendocardial myocardium with a complete but delayed filling and enhancement during the first pass. This delay of wash-in can be affected by the appearance of the DRA. This artifact mimics a true perfusion defect, impairing the images analysis (15,24,25). However, it can be recognized due to a different time course compared to a real perfusion defect, which tends to be visible for a longer duration (26). The DRA seems to be caused by a mixture of different factors and phenomena such as susceptibility (15), spatial resolution (Gibbs ringing) (16), and motion effects (17). In this work, we considered the contribution of spatial resolution and motion.

We performed perfusion experiments in six pigs by using two different resolutions (high and low) and two different heart rates (normal and tachycardia), resulting in four distinct experiment groups, tested for differences

Table 1
Comparison of Mean Signal Drop and Width of the Dark Rim Among the Three Myocardial Slices in Each Identified Group

| Groups	Parameters	Slices			*P*
		Apical	Medium	Basal	
HRes-rest	Signal drop (%)	20.0 ± 13.4	22.6 ± 14.9	20.1 ± 10.1	ns
	Width of rim (%)	6.5 ± 7.9	6.3 ± 4.7	7.8 ± 6.8	ns
	Width of rim (mm)	0.43 ± 0.55	0.43 ± 0.30	0.56 ± 0.44	ns
HRes-tachycardia	Signal drop (%)	32.5 ± 10.5	31.9 ± 6.9	30.4 ± 7.1	ns
	Width of rim (%)	38.5 ± 10.1	42.6 ± 7.6	42.7 ± 4.7	ns
	Width of rim (mm)	2.22 ± 0.54	3.09 ± 1.16	3.27 ± 0.56	ns
LRes-rest	Signal drop (%)	31.7 ± 13.0	29.9 ± 6.7	34.7 ± 10.1	ns
	Width of rim (%)	45.1 ± 23.2	45.2 ± 13.4	47.9 ± 7.3	ns
	Width of rim (mm)	2.73 ± 1.69	3.10 ± 1.35	3.29 ± 0.86	ns
LRes-tachycardia	Signal drop (%)	40.4 ± 13.9	30.9 ± 8.3	34.6 ± 11.5	ns
	Width of rim (%)	69.3 ± 17.5	66.3 ± 21.7	62.8 ± 9.5	ns
	Width of rim (mm)	5.57 ± 1.61	5.01 ± 1.37	4.88 ± 0.60	ns
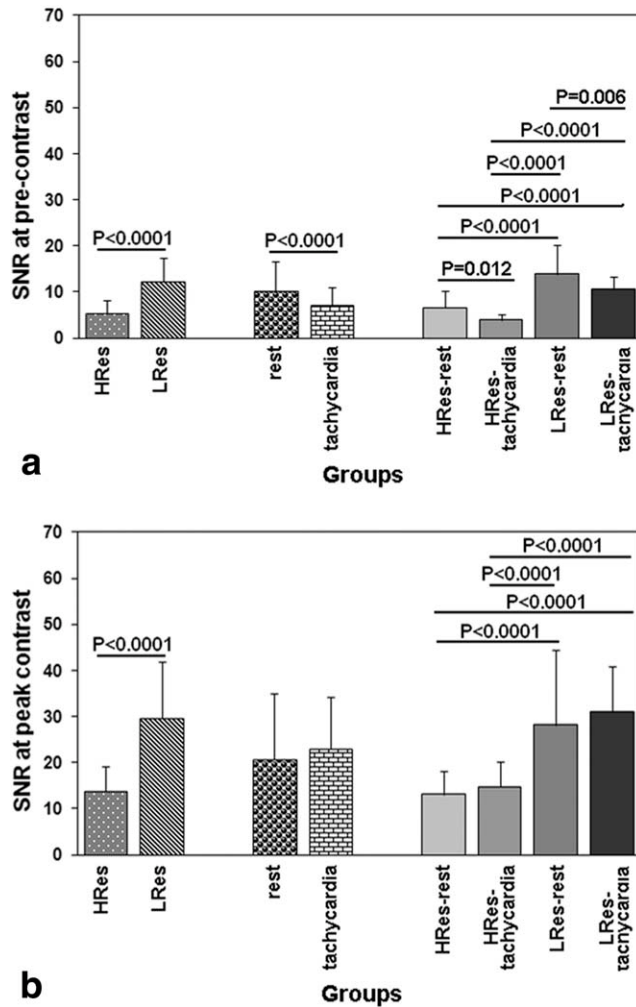
FIG. 5. **a**: SNR at precontrast in HRes and LRes groups (left), in normal and tachycardia groups (center) and in the four separate groups (right). **b**: SNR at peak contrast in HRes and LRes groups (left), in normal and tachycardia groups (center), and in the four separate groups (right). The SD is reported. The horizontal lines indicate a significant difference between two groups and the correspondent *P* values are indicated.

in signal drop and transmural extent of the dark-rim artifact. Moreover, we used a high-performance sequence: a gradient echo EPI sequence with a center out k-space filling and parallel imaging (ASSET) with a factor of 2. We obtained images of good quality in which it was always possible to characterize the artifact when present. The most prominent dark rim was identified on image frames shortly after the LV signal peak, when the contrast agent begun to perfuse the myocardium whereas the LV signal was still high (27).

From quantitative analysis of transmural myocardial signal profiles, we observed that the signal drop significantly increased with the heart rate, reflecting cardiac motion. This effect was more significant in the high-resolution images (Fig. 4a). It should be noted that the amplitude of the signal drop could be reduced by the partial volume effect, due to the small width of the dark rim (1–3 pixels). The partial volume effect is more prominent in

low-resolution images, making the amplitude of the signal drop not significantly different between high- and low-resolution images. The width of the DRA increased with decreased spatial resolution and with increased heart rate (Fig. 4b). The dark rim was significantly wider at high heart rates even with high-spatial resolution, demonstrating its dominant contribution to the occurrence of this artifact. This fact may have some implications in rest-stress studies. It may be possible that a "perfusion defect" on the stress images could be a DRA, even if there is not a dark-rim on the rest images. This may limit the specificity of perfusion imaging, highlighting the importance of continuing to improve pulse sequences for stress myocardial perfusion imaging.

Cardiac three-dimensional-motion can be described by three components: radial displacement, rotation, and translation (28). The direction of all these motion components changes each heart cycle during systole and diastole. At lower heart rates and at some phases of the heart cycle (mid diastole or, for an even shorter period, end-systole), the myocardium shows no or very little motion, whereas at other phases (systole, early diastole), the myocardium shows rapid motion. Furthermore, the motion of the myocardium shows largest and fastest excursion at the subendocardium at the basal segments (29,30,31). Changes in duration of the different phases of the heart cycle at high heart rates occur mainly in the diastolic phase. At high heart rates, early and end-diastolic motions merge resulting in nearly no motionless state (32,33). The normal range of myocardial thickness at end-diastole in adults is 9–10 mm. An in-plane spatial resolution >3 mm (as it is for a FOV of 40 and a matrix size of 128) results in the best case in no more than three pixels without any partial volume effects, and in the majority of cases, in two pixels without partial volume effects. This is even worse with the frequently used asymmetric matrix (such as 128×96),
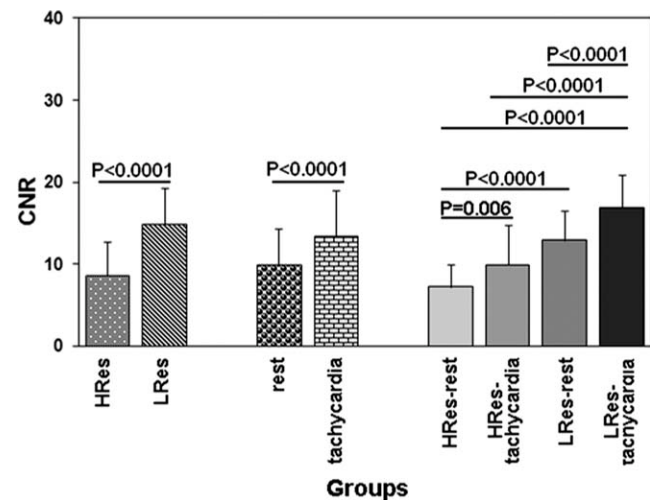

FIG. 6. CNR in HRes and LRes groups (left), in normal and tachycardia groups (center), and in the four separate groups (right). The SD is reported. The horizontal lines indicate a significant difference between two groups and the correspondent *P* values are indicated.

which results in in-plane rectangular pixels. In this case, no more than two pixels without partial volume effects can be present within the myocardial wall. Taking into account a myocardial motion up 7 cm/s, this could result in an artifact up to 1.5 cm width (17). Considering the normal myocardial thickness, the width of this calculated artifact would exceed the normal thickness of the myocardium. Depending on the heart phase and the extent of motion during that phase, the resulting artifact might cover the whole transmurality. This occurred in many cases in the present study, mainly at low spatial resolution and high heart rates, where the DRA covered the whole transmural extent of the myocardium in some segments.

No significant variation of the extension of the dark rim between the slices was observed in any of the four groups (Table 1), suggesting no preferential localization of the artifact.

It might be thought that the dark rim artefact represents just an optical illusion. In fact, a "dark" object (as the myocardium) that presents a convex contour relative to a concave surround at the interface with "bright" objects (as the LV) may produce a negative Mach band (34) that may mimic the dark rim artefact. The results allowed us to refuse this hypothesis.

Good SNR and CNR are prerequisites for the differentiation between normal and hypoperfused myocardium, especially for the detection of mild to moderate perfusion defects (35). All our images showed good SNR and CNR. As expected, the SNR and CNR ratios decreased with increasing spatial resolution (Figs. 5 and 6). The SNR and CNR in HRes-rest and HRes-tachycardia groups, characterized by high spatial resolution, were significantly lower than in LRes-rest and LRes-tachycardia groups. The SNR in the precontrast images was significantly higher in the LRes group compared to the HRes group. This pattern was not found in peak-contrast images. It should be noted that the dobutamine is associated with a twofold to threefold increase in coronary blood flow (36). An increased flow could cause a shorter T_1 and a higher SNR on the sequences with dobutamine-induced high heart rate.

The findings of this study suggest that several considerations should be made to reduce the dark rim. A cardiac perfusion sequence should demonstrate high-spatial resolution to minimize Gibbs ringing and high-temporal resolution to minimize motion artifacts. The design of a sequence for perfusion requires a compromise between spatial and temporal resolution. While spatial resolution should be kept as high as possible, the main target in an optimal sequence would be to reduce acquisition time as much as possible. The increase of the temporal resolution can be achieved by parallel imaging.

In conclusion, the DRA arises from a combination of different factors, and it can be diminished by reducing the acquisition time while keeping spatial resolution small. Both spatial and temporal resolutions are important determinants for the appearance of the artifact. The design of perfusion sequences should consider these variables to increase its diagnostic reliability.

REFERENCES

1. Wolff SD, Schwitter J, Coulden R, Friedrich MG, Bluemke DA, Biederman RW, Martin ET, Lansky AJ, Kashanian F, Foo TK, Licato PE, Comeau CR. Myocardial first-pass perfusion magnetic resonance imaging: a multicenter dose-ranging study. Circulation 2004;110: 732–737.
2. Maddahi J, Van Train K, Prigent F, Garcia EV, Friedman J, Ostrzega E, Berman D. Quantitative single photon emission computed thallium-201 tomography for detection and localization of coronary artery disease: optimization and prospective validation of a new technique. J Am Coll Cardiol 1989;14:1689–1699.
3. Hutchins GD, Schwaiger M, Rosenspire KC, Krivokapich J, Schelbert H, Kuhl DE. Noninvasive quantification of regional blood flow in the human heart using N-13 ammonia and dynamic positron emission tomographic imaging. J Am Coll Cardiol 1990;15:1032–1042.
4. Kuhle WG, Porenta G, Huang SC, Buxton D, Gambhir SS, Hansen H, Phelps ME, Schelbert HR. Quantification of regional myocardial blood flow using 13N-ammonia and reoriented dynamic positron emission tomographic imaging. Circulation 1992;86:1004–1017.
5. Hesse B, Tagil K, Cuocolo A, Anagnostopoulos C, Bardies M, Bax J, Bengel F, Busemann Sokole E, Davies G, Dondi M, Edenbrandt L, Franken P, Kjaer A, Knuuti J, Lassmann M, Ljungberg M, Marcassa C, Marie PY, McKiddie F, O'Connor M, Prvulovich E, Underwood R, van Eck-Smit B. EANM/ESC procedural guidelines for myocardial perfusion imaging in nuclear cardiology. Eur J Nucl Med Mol Imaging 2005;32:855–897.
6. Schwaiger M. Myocardial perfusion imaging with PET. J Nucl Med 1994;35:693–698.
7. Go RT, Marwick TH, MacIntyre WJ, Saha GB, Neumann DR, Underwood DA, Simpfendorfer CC. A prospective comparison of rubidium-82 PET and thallium-201 SPECT myocardial perfusion imaging utilizing a single dipyridamole stress in the diagnosis of coronary artery disease. J Nucl Med 1990;31:1899–1905.
8. Manning WJ, Atkinson DJ, Grossman W, Paulin S, Edelman RR. First-pass nuclear magnetic resonance imaging studies using gadolinium-DTPA in patients with coronary artery disease. J Am Coll Cardiol 1991;18:959–965.
9. Bruder O, Schneider S, Nothnagel D, Dill T, Hombach V, Schulz-Menger J, Nagel E, Lombardi M, van Rossum AC, Wagner A, Schwitter J, Senges J, Sabin GV, Sechtem U, Mahrholdt H. EuroCMR (European Cardiovascular Magnetic Resonance) registry: results of the German pilot phase. J Am Coll Cardiol 2009;54:1457–1466.
10. Miller DD, Holmvang G, Gill JB, Dragotakes D, Kantor HL, Okada RD, Brady TJ. MRI detection of myocardial perfusion changes by gadolinium-DTPA infusion during dipyridamole hyperemia. Magn Reson Med 1989;10:246–255.
11. Schaefer S, Lange RA, Gutekunst DP, Parkey RW, Willerson JT, Peshock RM. Contrast-enhanced magnetic resonance imaging of hypoperfused myocardium. Invest Radiol 1991;26:551–556.
12. Wagner A, Mahrholdt H, Holly TA, Elliott MD, Regenfus M, Parker M, Klocke FJ, Bonow RO, Kim RJ, Judd RM. Contrast-enhanced MRI and routine single photon emission computed tomography (SPECT) perfusion imaging for detection of subendocardial myocardial infarcts: an imaging study. Lancet 2003;361:374–379.
13. Sakuma H, Suzawa N, Ichikawa Y, Makino K, Hirano T, Kitagawa K, Takeda K. Diagnostic accuracy of stress first-pass contrast-enhanced myocardial perfusion MRI compared with stress myocardial perfusion scintigraphy. AJR Am J Roentgenol 2005;185:95–102.
14. Ishida N, Sakuma H, Motoyasu M, Okinaka T, Isaka N, Nakano T, Takeda K. Noninfarcted myocardium: correlation between dynamic first-pass contrast-enhanced myocardial MR imaging and quantitative coronary angiography. Radiology 2003;229:209–216.
15. Barkhausen J, Hunold P, Jochims M, Debatin JF. Imaging of myocardial perfusion with magnetic resonance. J Magn Reson Imaging 2004; 19:750–757.
16. Di Bella EV, Parker DL, Sinusas AJ. On the dark rim artifact in dynamic contrast-enhanced MRI myocardial perfusion studies. Magn Reson Med 2005;54:1295–1299.
17. Storey P, Chen Q, Li W, Edelman RR, Prasad PV. Band artifacts due to bulk motion. Magn Reson Med 2002;48:1028–1036.
18. Kellman P, Arai AE. Imaging sequences for first pass perfusion—a review. J Cardiovasc Magn Reson 2007;9:525–537.
19. Positano V, Pingitore A, Scattini B, Santarelli MF, De Marchi D, Favilli B, Lombardi M, Landini L. Myocardial perfusion by first pass

contrast magnetic resonance: a robust method for quantitative regional assessment of perfusion reserve index. Heart 2006;92:689–690.

20. Positano V, Santarelli MF, Landini L. Automatic characterization of myocardial perfusion in contrast enhanced MRI. EURASIP J Appl Signal Process 2003;2003:413–421.

21. Gudbjartsson H, Patz S. The Rician distribution of noisy MRI data. Magn Reson Med 1995;34:910–914.

22. Constantinides CD, Atalar E, McVeigh ER. Signal-to-noise measurements in magnitude images from NMR phased arrays. Magn Reson Med 1997;38:852–857.

23. Al-Saadi N, Nagel E, Gross M, Bornstedt A, Schnackenburg B, Klein C, Klimek W, Oswald H, Fleck E. Noninvasive detection of myocardial ischemia from perfusion reserve based on cardiovascular magnetic resonance. Circulation 2000;101:1379–1383.

24. Lyne JC, Gatehouse PD, Assomull RG, Smith GC, Kellman P, Firmin DN, Pennell DJ. Direct comparison of myocardial perfusion cardiovascular magnetic resonance sequences with parallel acquisition. J Magn Reson Imaging 2007;26:1444–1451.

25. Weber S, Kronfeld A, Kunz RP, Fiebich M, Horstick G, Kreitner KF, Schreiber WG. Comparison of three accelerated pulse sequences for semiquantitative myocardial perfusion imaging using sensitivity encoding incorporating temporal filtering (TSENSE). J Magn Reson Imaging 2007;26:569–579.

26. Arai AE. Magnetic resonance first-pass myocardial perfusion imaging. Top Magn Reson Imaging 2000;11:383–398.

27. Ferreira P, Gatehouse P, Kellman P, Bucciarelli-Ducci C, Firmin D. Variability of myocardial perfusion dark rim Gibbs artifacts due to sub-pixel shifts. J Cardiovasc Magn Reson 2009;27:11:17.

28. Reichek N. MRI myocardial tagging. J Magn Reson Imaging 1999;10:609–616.

29. Lionetti V, Guiducci L, Simioniuc A, Aquaro GD, Simi C, De Marchi D, Burchielli S, Pratali L, Piacenti M, Lombardi M, Salvadori P, Pingitore A, Neglia D, Recchia FA. Mismatch between uniform increase in cardiac glucose uptake and regional contractile dysfunction in pacing-induced heart failure. Am J Physiol Heart Circ Physiol 2007;293:H2747–2756.

30. Reant P, Labrousse L, Lafitte S, Bordachar P, Pillois X, Tariosse L, Bonoron-Adele S, Padois P, Deville C, Roudaut R, Dos Santos P. Experimental validation of circumferential, longitudinal, and radial 2-dimensional strain during dobutamine stress echocardiography in ischemic conditions. J Am Coll Cardiol 2008;51:149–157.

31. Pirat B, Khoury DS, Hartley CJ, Tiller L, Rao L, Schulz DG, Nagueh SF, Zoghbi WA. A novel feature-tracking echocardiographic method for the quantitation of regional myocardial function: validation in an animal model of ischemia-reperfusion. J Am Coll Cardiol 2008;51:651–659.

32. Poerner TC, Goebel B, Geiger T, Haghi D, Borggrefe M, Haase KK. Physiological range of mechanical synchronicity of the human heart: comparison between different echocardiographic assessment modalities. Ultrasound Med Biol 2005;31:1163–1172.

33. Notomi Y, Popovic ZB, Yamada H, Wallick DW, Martin MG, Oryszak SJ, Shiota T, Greenberg NL, Thomas JD. Ventricular untwisting: a temporal link between left ventricular relaxation and suction. Am J Physiol Heart Circ Physiol 2008;294:H505–H513.

34. Chansen Lauerma K, Virtanen KS, Sipila LM, Hekali P, Aronen HJ. Multislice MRI in assessment of myocardial perfusion in patients with single-vessel proximal left anterior descending coronary artery disease before and after revascularization. Circulation 1997;96:2859–2867.

35. Lauerma K, Virtanen KS, Sipila LM, Hekali P, Aronen HJ. Multislice MRI in assessment of myocardial perfusion in patients with single-vessel proximal left anterior descending coronary artery disease before and after revascularization. Circulation 1997;96:2859–2867.

36. Jagathesan R, Barnes E, Rosen SD, Foale R, Camici PG. Dobutamine-induced hyperaemia inversely correlates with coronary artery stenosis severity and highlights dissociation between myocardial blood flow and oxygen consumption. Heart 2006;92:1230–1237.